

# Catalysis Science & Technology

Accepted Manuscript



This is an *Accepted Manuscript*, which has been through the Royal Society of Chemistry peer review process and has been accepted for publication.

*Accepted Manuscripts* are published online shortly after acceptance, before technical editing, formatting and proof reading. Using this free service, authors can make their results available to the community, in citable form, before we publish the edited article. We will replace this *Accepted Manuscript* with the edited and formatted *Advance Article* as soon as it is available.

You can find more information about *Accepted Manuscripts* in the [Information for Authors](#).

Please note that technical editing may introduce minor changes to the text and/or graphics, which may alter content. The journal's standard [Terms & Conditions](#) and the [Ethical guidelines](#) still apply. In no event shall the Royal Society of Chemistry be held responsible for any errors or omissions in this *Accepted Manuscript* or any consequences arising from the use of any information it contains.



[www.rsc.org/catalysis](http://www.rsc.org/catalysis)



Journal Name

ARTICLE

## Promoter effect of potassium in CuO/CeO<sub>2</sub> systems supported on carbon nanotubes and graphene for the CO-PROX reaction

A.B. Dongil<sup>\*a</sup>, B. Bachiller-Baeza<sup>\*b,c</sup>, E. Castillejos<sup>d</sup>, N. Escalona<sup>e,f</sup>, A. Guerrero-Ruiz<sup>c,d</sup> and I. Rodríguez-Ramos<sup>b,c</sup>

Received 00th January 20xx,  
Accepted 00th January 20xx

DOI: 10.1039/x0xx00000x

www.rsc.org/

The effect of K promotion on the CO preferential oxidation (CO-PROX) reaction has been studied over Cu-CeO<sub>2</sub> based catalysts supported on carbon nanotubes (CNT) and reduced graphene oxide (G). The catalysts were prepared with 3 wt % Cu and 20 wt % CeO<sub>2</sub> loadings, and 1 wt % K when promoted. In the CNT series, K loading was varied between 0.5 and 2 wt %. The catalytic performance and the characterization by powder X-ray diffraction (XRD), TEM-STEM, H<sub>2</sub>-temperature-programmed reduction (H<sub>2</sub>-TPR) and X-ray photoelectron spectroscopy (XPS) has been presented. TEM analysis showed that the type of carbon support has an important effect on the dispersion of ceria, this latter being higher for CNT support. Addition of K to the catalysts improved the conversion of CO at lower temperatures. The characterization results reveal that the observed increase in the Cu<sup>+</sup> species proportion and in lattice oxygen are related to the better catalytic performance.

### Introduction

The selective oxidation of carbon monoxide employing a small amount of O<sub>2</sub> (CO-PROX), is considered one of the best alternatives to purify the hydrogen rich stream obtained from the hydrocarbon reforming and subsequent WGS reaction. The CO amount has to be reduced to levels lower than 10 ppm in order to avoid the poisoning of the Pt-based electrodes which are employed on the proton exchange membranes of fuel cells, where H<sub>2</sub> is used as fuel.<sup>1</sup> Several catalytic systems have been explored for CO-PROX reaction, among them the CuO-CeO<sub>2</sub> based-catalysts proved to exhibit good results in terms of activity and selectivity, while having a lower price compared to noble metals-based catalysts.<sup>2</sup> According to several studies, the interface of CuO-CeO<sub>2</sub> is responsible of its catalytic performance. It has been revealed that the active sites for CO-PROX reaction are Cu<sup>+</sup> entities, which are formed after reduction by contact with the feed mixture and promoted by ceria. The reaction takes place over those Cu<sup>+</sup> sites where the

CO molecules adsorb.<sup>3,4</sup> Ceria can promote the mobility of surface oxygen species over the catalyst surface due to the Ce<sup>+4</sup> ↔ Ce<sup>+3</sup> redox process, this favouring the Cu<sup>+</sup> ↔ Cu<sup>+2</sup> reaction.<sup>5</sup> In addition, ceria can stabilize small metal nanoparticles.<sup>5,6</sup>

In order to improve the efficiency and stability of CuO-CeO<sub>2</sub> systems, several alternatives have been considered<sup>7</sup>. Mixed oxides CeO<sub>2</sub>-MO<sub>x</sub><sup>8,9,10</sup> or doping elements as Mn or Fe<sup>11,12,13</sup> have been studied with different results. The addition of TiO<sub>2</sub> increases the surface area and reduces the particle size<sup>8</sup> and, similarly, ZrO<sub>2</sub> improved CuO dispersion and its interaction with CeO<sub>2</sub>, which was ascribed to the disorder and defects induced by the presence of zirconia.<sup>10</sup> On the other hand, the addition of Mn<sub>x</sub>O<sub>2</sub> seems to increase the lattice oxygen mobility,<sup>9</sup> while small amounts of Mn and Fe enhance the CuO-CeO<sub>2</sub> interaction and the oxygen vacancies.<sup>11,13</sup>

Increasing the amount of defects sites of ceria would increase the formation of oxygen vacancies and, thus, the Cu reducibility would be enhanced. As the defects sites are mainly located on the external surface, reducing the particle size of ceria would increase the number of defects and this can be achieved, for example, by supporting CuO-CeO<sub>2</sub> onto a high surface area support.<sup>14</sup> Supporting ceria, will also allow to use a smaller amount of this low available oxide. In this sense, it is has been studied the positive effect of dispersing Pt-CeO<sub>2</sub> over carbon nanotubes compared to a traditional support as activated carbon,<sup>15</sup> the effect of the CuO loading over CeO<sub>2</sub>/CNT<sup>16</sup> and the different catalytic behaviour by preferential location of the active phase inside or outside the CNT.<sup>17</sup> Besides their mesoporous structure and special morphology as rolling graphene layers, carbon nanotubes can offer peculiar electronic, adsorption, mechanical and thermal

<sup>a</sup> Universidad de Concepción, Departamento de Físicoquímica, Laboratorio de Catálisis por metales, Edmundo Larenas 129, Concepción, Chile. E-mail: adongil@udec.cl

<sup>b</sup> Instituto de Catálisis y Petroleoquímica, CSIC, c/Marie Curie No. 2, Cantoblanco, 28049 Madrid, Spain. E-mail: b.bachiller@icp.csic.es

<sup>c</sup> Grupo de Diseño y Aplicación de Catalizadores Heterogéneos, Unidad Asociada UNED-CSIC (ICP), Spain.

<sup>d</sup> Dpto. Química Inorgánica y Técnica, Fac. de Ciencias, UNED, C/ Senda del Rey n° 9, 28040, Madrid, Spain.

<sup>e</sup> Departamento de Ingeniería Química y Bioprocesos, Pontificia Universidad Católica de Chile, Avda. Vicuña Mackenna 4860, Macul, Santiago, Chile.

<sup>f</sup> Facultad de Químicas, Pontificia Universidad Católica de Chile.

Electronic Supplementary Information (ESI) available: [details of any supplementary information available should be included here]. See DOI: 10.1039/x0xx00000x

properties.<sup>18</sup> Since the reaction mechanism involves the formation of oxygen vacancies and the above mentioned redox process, it is expected that the addition of an element that can enhance the oxygen mobility, would have a positive effect on the reaction. Alkali metals have been employed as promoter for CeO<sub>2</sub>-based catalyst and it has been observed that when they are incorporated in the CeO<sub>2</sub> lattice, some changes are induced in the ceria structure that can improve the reducibility of the catalyst.<sup>19,20</sup> Moreover, the promotion with alkalis can prevent the formation of coke deposits and decrease the reduction temperature of the metal oxides. However, the investigations on the effects of alkali promotion on CO-PROX have been scarce and mainly on noble metal-based catalysts.<sup>21-23</sup> In general, the addition of alkali or alkali earth metal cations brings about up to a 10-fold enhancement in the low temperature PROX activity. Its promotional effect has been related to electronic effects or the creation of reaction OH groups that react smoothly with CO adsorbed on neighbouring metal atoms as in Pt to give CO<sub>2</sub> as the product.

Therefore, in the present work we studied the promoter effect of potassium over Cu-CeO<sub>2</sub>/CNT and over an analogous system supported over a lab-prepared graphene to study the influence of the support morphology. The best support was used to study the influence of potassium loading.

## Experimental

### Catalyst preparation

Commercial carbon nanotubes (Nanocyl 3100, > 95% purity, CNT) and a lab-prepared reduced graphene oxide, G, were used as starting supports. This reduced graphene oxide was prepared from a graphite oxide synthesized using a modified Brodie's method and the subsequent exfoliation at 723 K in N<sub>2</sub> atmosphere.<sup>24</sup> For the cerium precursor impregnation, the corresponding amount of Ce(NO<sub>3</sub>)<sub>3</sub>·6H<sub>2</sub>O (99.99%, Sigma-Aldrich) to obtain a 20 wt % was dissolved in acetone. The CNT was added to the solution, in a proportion of 10 mL/g of support, with stirring. After 6 h in a covered flask, the excess of solvent was slowly removed in a rotator evaporator under vacuum, until complete removal of the solvent. The solid was dried for 24 h at 373 K and finally, it was heat treated during 5 h at 623 K under flowing nitrogen (50 mL/min), with a heating rate of 1 K min<sup>-1</sup>. In this way the samples CeO<sub>2</sub>/CNT and CeO<sub>2</sub>/G were obtained. The Cu catalysts were prepared by dissolving in acetone (10 mL of solution per gram of solid) the proper amount of Cu(NO<sub>3</sub>)<sub>2</sub>·3H<sub>2</sub>O (99.9%, Sigma-Aldrich) and KNO<sub>3</sub> (≥ 99.9% Sigma-Aldrich). After stirring for 6 h, the solvent was removed under vacuum at 333 K and the solid was dried for 24 h at 373 K. Finally, the materials were treated at 623 K for 5 h under flowing nitrogen (50 mL min<sup>-1</sup>). The amount of CuO was fixed to 3 wt % and the amount of K on the CeO<sub>2</sub>/CNT was varied to obtain 0.5 wt % (K0.5), 1.0 wt % (K1), 1.5 wt % (K1.5) and 2.0 wt % (K2). According to this procedure five catalysts were prepared which are labelled as Cu-CeO<sub>2</sub>/CNT, and Cu(Kx)-CeO<sub>2</sub>/CNT. Cu-CeO<sub>2</sub>/G and Cu(K1)-

CeO<sub>2</sub>/G were also prepared in a similar way. For the sake of comparison, Cu/CNT was synthesized in a similar way.

### Techniques for characterisation

Powder X-ray diffraction (XRD) patterns of the samples were obtained on a Polycrystal X'Pert Pro Analytical diffractometer with Ni-filtered Cu K $\alpha$  radiation ( $\lambda=0.1542$  nm) operating at 45 kV and 40 mA. For each sample, Bragg's angles between 4 and 90 ° were scanned with steps of 0.04 °.

Temperature-programmed reduction (TPR) measurements were carried out in a U-shaped quartz cell using a 5% H<sub>2</sub>/He gas flow of 25 cm<sup>3</sup> min<sup>-1</sup> and about 0.15 g of sample, with a heating rate of 10 K min<sup>-1</sup> (TPR/TPD2900 Micromeritics system). Hydrogen consumption was followed by on-line gas-chromatograph (TCD).

Transmission electron microscopy (TEM) and annular dark-field scanning transmission electron microscopy (ADF-STEM) images were measured using a JEOL JEM 2100F field emission electron gun microscope operated at 200 kV and equipped with an energy-dispersive X-ray detector. The samples were ground and a small amount was suspended in ethanol solution using an ultrasonic bath. Some drops were added to the nickel grid (Aname, Lacey carbon 200 mesh) and the ethanol was evaporated at room temperature before introduce in the microscope. The imaging in the scanning transmission electron microscopy (STEM) mode was done using a spot size of 1 nm. X-ray energy dispersive spectroscopic (EDS) mapping analysis was carried out with the help of an Oxford Instruments Inca software package.

X-ray photoelectron spectra of the fresh samples were recorded with an ESCAPROBE P spectrometer from Omicron equipped with an EA-125 hemi-spherical electron multichannel analyser and X-ray source (Mg K $\alpha$ ) operated at 150 W, with pass energy of 50 eV. Each sample was pressed into a small pellet of 15 mm diameter and placed in the sample holder and degassed in the chamber for 6–8 h to achieve a dynamic vacuum below 10<sup>-8</sup> Pa before analysis. The spectral data for each sample was analyzed using CASA XPS software. The binding energy is referenced to the C 1s line at 284.6 eV. The relative concentrations and atomic ratios were determined from the integrated intensities of photoelectron lines corrected for the corresponding atomic sensitivity factor.

### Catalytic measurements

The CO-PROX reaction was studied in a fix-bed reactor under atmospheric pressure and temperatures in the range 323-473 K. The activity tests were performed using 0.050 g of catalyst. The catalysts were directly exposed to reaction gas without any pretreatment. A mixture of 1% CO, 1% O<sub>2</sub>, 50% H<sub>2</sub> (He balance) at a total flow rate of 100 ml min<sup>-1</sup> was passed through the catalytic bed. The composition of the gas stream exiting the reactor was determined with a Varian CP-3380 gas chromatograph equipped with a TCD detector and a CarboxenTM-1000 (15 ft × 1/8 in) column.

The conversion of CO ( $C_{CO}$ ) and the selectivity towards  $CO_2$  ( $S_{CO_2}$ ) were calculated as shown in Equations (1) and (2),

$$C_{CO} (\%) = \frac{[CO]_{in} - [CO]_{out}}{[CO]_{in}} \times 100 \quad (1)$$

$$S_{CO_2} (\%) = 0.5 \times \frac{[CO]_{in} - [CO]_{out}}{[O_2]_{in} - [O_2]_{out}} \times 100 \quad (2)$$

## Results and discussion

### Catalysts characterization

The XRD patterns of the catalysts are shown in Figure 1. For the CNT-based catalysts, besides the diffractions peaks at  $26.1^\circ$  and  $43.1^\circ$  corresponding to the hkl reflections (002) and (100) of graphite, the characteristic  $CeO_2$  peaks at  $28.6^\circ$ ,  $33.4^\circ$ ,  $47.8^\circ$  and  $56.7^\circ$ , due to the reflections in the (111), (200), (220) and (331) crystalline planes of the cubic fluorite type phase (JCPDS 34-0394), can be clearly observed. The intensity and wideness of the diffractions can be taken as an indication of the crystallinity. The XRD profile of  $CeO_2/G$  displayed the narrowest peaks among the samples, indicating a high crystallinity and suggesting larger particle size in agreement with the microscopy (see later). The mean crystallite sizes of  $CeO_2$  were estimated by application of the Scherrer equation to the (220) diffraction peak and are shown in Table 1. This reflection was selected due to the interference of carbon supports in the (111) and (200) reflections. It is noted that the diffraction peaks due to  $CuO$ ,  $Cu_2O$  or  $Cu$  were not detected in  $Cu-CeO_2/CNT$ ,  $Cu-CeO_2/G$  catalysts, which may be related to the low amount of  $Cu$ , the formation of extremely small clusters well dispersed on the surface or to the incorporation of  $Cu$  into the ceria lattice. It is also remarkable the increase of  $CeO_2$  dispersion on  $Cu-CeO_2/G$  catalysts compared to the original  $CeO_2/G$ . In a similar fashion, only diffractions ascribed to ceria could be observed for the K-promoted sample,  $Cu(K1)-CeO_2/CNT$  and  $Cu(K1)-CeO_2/G$ . The crystallite size presented similar values to that of the potassium-free catalyst  $Cu-CeO_2/CNT$ ,  $Cu-CeO_2/G$ .

Table 1. Mean crystallite sizes of  $CeO_2$  determined by XRD

Catalyst	d (nm)
$CeO_2/CNT$	6.1
$Cu-CeO_2/CNT$	4.3
$Cu(K1)-CeO_2/CNT$	4.2
$CeO_2/G$	11.6
$Cu-CeO_2/G$	3.4
$Cu(K1)-CeO_2/G$	4.0

Selected TEM and HRTEM images of the calcined samples  $CeO_2/CNT$  and  $CeO_2/G$  are shown in Figures 2 and 3. Figure 2a for  $CeO_2/CNT$  sample showed that ceria was mainly wrapped around the nanotubes as aggregates of multiple small particles whose estimated particle size was around 5 nm, consistent with the crystallite size determined by XRD. The lattice fringes

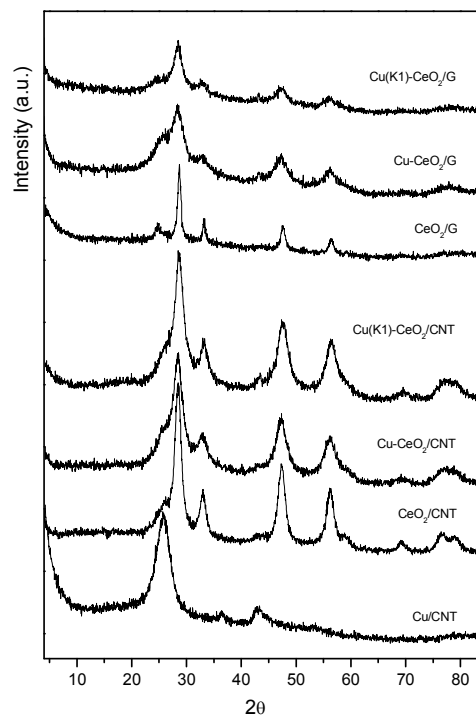


Figure 1. XRD patterns of CNT- and graphene-supported samples.

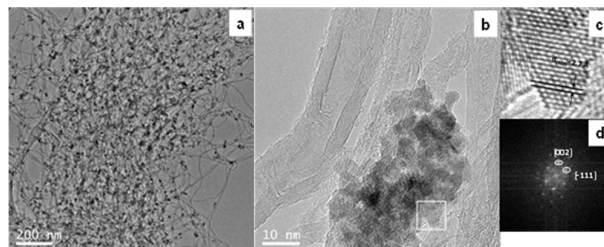


Figure 2. (a) and (b) Representative TEM and HRTEM images of  $CeO_2/CNT$  sample, (c) zoom of the highlighted area in (b) showing lattice fringes and (d) FFT for  $CeO_2$  phase.

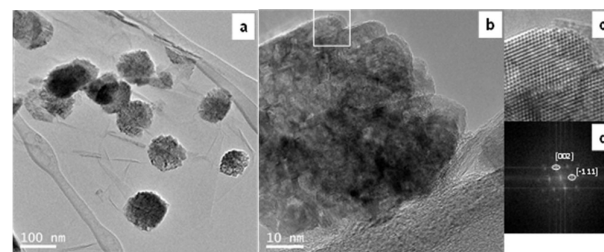


Figure 3. (a) and (b) Representative TEM and HRTEM images of  $CeO_2/G$  sample, (c) zoom of the highlighted area in (b) showing lattice fringes, and (d) FFT for  $CeO_2$  phase.

whose interplanar distances of ca. 2.71 and 3.12 nm (Figure 2c) indexed to the (200) and (111) planes of the cubic ceria, and the corresponding FFT (Figure 2d) indicated that the ceria phase was along the [100] axis of the fluorite structure. The large graphene sheets of CeO<sub>2</sub>/G sample can be clearly observed in Figure 3a. CeO<sub>2</sub> is present on this sample as circumscribed round-shaped nanoparticles on the surface with a roughly estimated average particle size of 70 nm. As occurred for CeO<sub>2</sub>/CNT sample, the lattice spacings and the FFT indicated the good crystallinity of the phase.

As long as the Cu-CeO<sub>2</sub>/CNT and Cu-CeO<sub>2</sub>/G samples are concerned, some differences can be envisaged in Figures 4a and 4b. In general, the same faces as those observed for the Cu-free CeO<sub>2</sub>/CNT sample appear exposed at the surface of the ceria crystals in the Cu-containing catalysts. For Cu-CeO<sub>2</sub>/G, a clear redispersion of the nanoparticles seemed to occur, consistent with the XRD data. In the dispersed aggregates, no copper-containing phase could however be resolved in any of the multiple HRTEM images taken for these samples. Promotion of the catalysts with K, Cu(K1)-CeO<sub>2</sub>/CNT (Figure 4c) and Cu(K1)-CeO<sub>2</sub>/G (Figure 4d), produced similar CeO<sub>2</sub> crystallites distributions.

The CO oxidation reaction is dependent on the redox properties of the catalysts. Herein, H<sub>2</sub>-TPR analysis was performed to gain the information about the reducibility and the chemical state of copper species of the as-prepared Cu-CeO<sub>2</sub>/CNT samples. Figure 5 shows the TCD signal evolution of H<sub>2</sub> consumption as a function of temperature for the carbon supported copper-ceria catalysts. As reference the profile for Cu/CNT sample is also listed. It can be seen that only one peak centred at around 490 K was observed in the pure Cu/CNT sample that was synthesized using a conventional impregnation method. As it is well known, the reduction

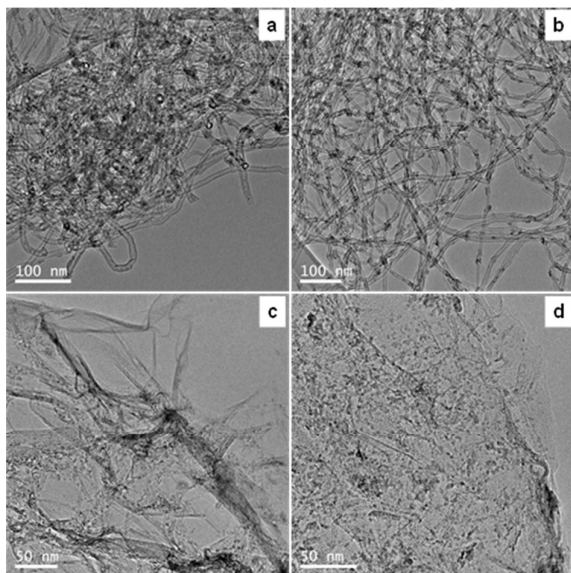


Figure 4. Representative TEM images of (a) Cu-CeO<sub>2</sub>/CNT, (b) Cu(K1)-CeO<sub>2</sub>/CNT, (c) Cu-CeO<sub>2</sub>/G and (d) Cu(K1)-CeO<sub>2</sub>/G samples.

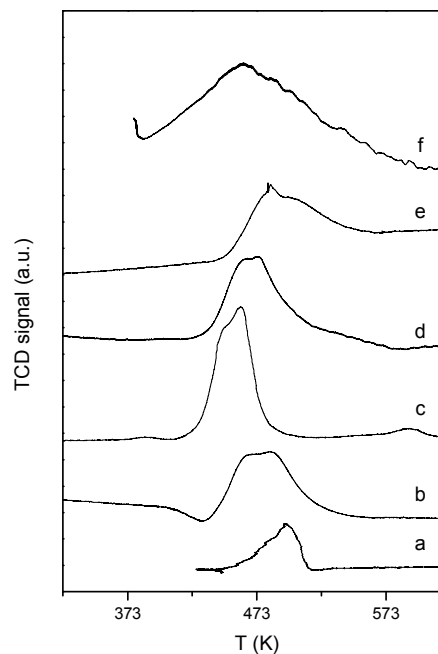


Figure 5. H<sub>2</sub>-TPR profiles of the catalysts: a) Cu/CNT, b) Cu-CeO<sub>2</sub>/CNT, c) Cu(K1)-CeO<sub>2</sub>/CNT, d) Cu(K2)-CeO<sub>2</sub>/CNT, e) Cu-CeO<sub>2</sub>/G, f) Cu(K1)-CeO<sub>2</sub>/G.

profile of pure CuO is characterized by a single peak at about 653 K.<sup>25,26</sup> As shown in Figure 5, the wide H<sub>2</sub>-TPR reduction peak of Cu-CeO<sub>2</sub>/CNT sample was located at ~478 K and presents two overlapping contributions,  $\alpha$  and  $\beta$ . A qualitative attribution of the TPR peaks to different Cu species over CeO<sub>2</sub> support has been proposed by many researchers.<sup>4,26-30</sup> In this work, based on the literature data and the above XRD and TEM results, the lower temperature reduction peak  $\alpha$  can be ascribed to finely dispersed CuO strongly interacting with CeO<sub>2</sub> and the higher temperature reduction peak  $\beta$  to bigger clusters of CuO weakly associated with the CeO<sub>2</sub>. Compared with the reduction of Cu/CNT, the decrease in the reduction temperature of Cu species in the prepared Cu-CeO<sub>2</sub>/CNT sample is consistent with the highly dispersed nature of the copper particles and can reveal the interaction between the CuO species and the CeO<sub>2</sub>, this facilitating the reduction of CuO. With the addition of K, Cu(K1)-CeO<sub>2</sub>/CNT sample, the peaks  $\alpha$  and  $\beta$  coalesced, since the peak was sharper. Furthermore, the peak was shifted to lower temperature, indicating that the presence of K favours the reduction of Cu.

By comparison of the TPR profiles between Cu-CeO<sub>2</sub>/CNT and Cu-CeO<sub>2</sub>/G it can be deduced that an effect of the support exists. The reduction of Cu is facilitated in the case of the CNT probably due to the higher interaction with the CeO<sub>2</sub> favoured by the smaller particle size, and an electron transfer from the CNT. For Cu-CeO<sub>2</sub>/G the wide peak and the presence of a contribution at 513 K, a temperature similar to that previously

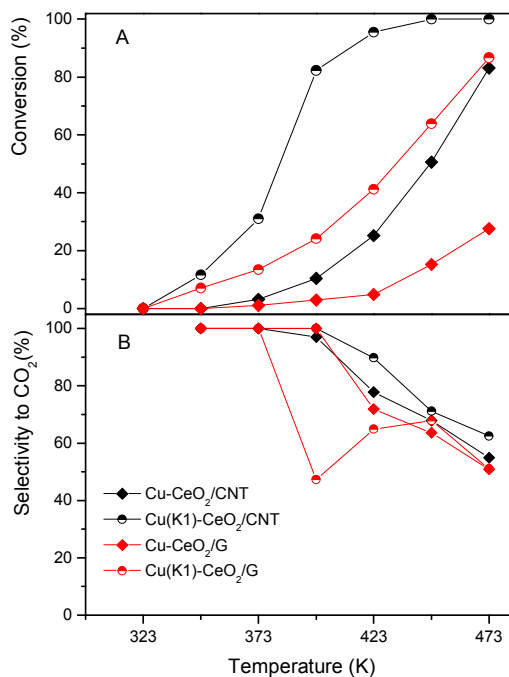


Figure 6. Plots of (A) CO conversion and (B) CO<sub>2</sub> selectivity versus temperature of CO-PROX reaction of non-promoted and K-promoted catalysts supported on CNT and G. Reaction conditions as indicated in the Experimental section, CO/O<sub>2</sub> = 1.

reported,<sup>27,30,31</sup> indicates that small segregated CuO clusters with no specific structure and probably over the carbon support are present. Addition of K on the graphene supported catalyst resulted in a widening of the peak and shifting to lower temperatures, similarly to the changes observed for the CNT samples.

#### PROX reaction

Figure 6 displays the catalytic activity in terms of CO conversion, and the selectivity to CO<sub>2</sub> as a function of temperature of the different Cu catalysts supported on the two carbon materials with and without potassium. It can be observed that all the catalysts were active except Cu/CNT, this confirming the important role of ceria. An effect of the support on the ceria dispersion and on the Cu-Ce interaction was clearly observed. The conversion obtained with the Cu-CeO<sub>2</sub>/CNT catalyst was higher than that reached with Cu-CeO<sub>2</sub>/G (30% conversion at 473 K). The catalytic activity was similar than that reported for comparable systems under similar reactions conditions.<sup>16,17</sup> The good dispersion of ceria over the CNT support, as observed by XRD and TEM, favoured the Cu-ceria interaction and thereby the reduction, as confirmed by H<sub>2</sub>-TPR experiments. On the other hand, the worse activity offered by the Cu-CeO<sub>2</sub>/G sample contrasts with the good dispersion observed by TEM. However, the higher

reduction temperature in the H<sub>2</sub>-TPR profile would be in line with a low proportion of Cu-Ce interacting which could be consequence of the larger ceria agglomerates of the initial CeO<sub>2</sub>/G sample (Figure 3). It can be seen that addition of K enhances the conversion values at lower temperatures over all the support materials. Moreover, the results show that Cu(K1)-CeO<sub>2</sub>/CNT exhibited the best activity among the compared catalysts. Additional elemental mapping analyses from the corresponding STEM-EDS data, Cu(K1)-CeO<sub>2</sub>/CNT (Figure 7) and Cu(K1)-CeO<sub>2</sub>/G (Figure 8), seem to confirm the homogeneous distribution of both Cu and Ce atoms, implying that copper may be well-dispersed on the samples or embedded in the lattice of ceria which can produce oxygen vacancies. Furthermore, some isolated domains or patches of copper phases are evident (ESI, Figure S1), which is in contrast to the related XRD results. A low proportion of Cu patches on the sample can explain this discrepancy. Although K was difficult to detect by EDS analysis most likely due to the low amount of the dopant, it can be clearly detected in areas where the Cu-CeO<sub>2</sub> nanoparticles are more aggregated (Figure 8b).

Therefore, based on the comparison among supports, the effect of potassium loading was studied by preparing a series of catalysts using CNT as parent support, Cu(K0.5)-CeO<sub>2</sub>/CNT, Cu(K1)-CeO<sub>2</sub>/CNT, Cu(K1.5)-CeO<sub>2</sub>/CNT and Cu(K2)-CeO<sub>2</sub>/CNT. In Figure 9 the reaction temperature dependence of CO conversion and selectivity to CO<sub>2</sub> over the potassium-promoted Cu-CeO<sub>2</sub>/CNT series are shown. All the samples were active from very low temperatures, i.e. 353 K. However, differences were observed as the K loading was varied. Initially, as the K loading increases from 0 to 1.5%, the conversion increases, reaching 97% at 423 K for Cu(K1)-CeO<sub>2</sub>/CNT and Cu(K1.5)-CeO<sub>2</sub>/CNT. Further increment in K content up to 2% resulted in a change of the tendency and the conversion decreased to 75%, a value similar to those of Cu(K0.5)-CeO<sub>2</sub>/CNT. In summary, the activity followed the trend: Cu(K1)-CeO<sub>2</sub>/CNT > Cu(K1.5)-CeO<sub>2</sub>/CNT > Cu(K0.5)-CeO<sub>2</sub>/CNT ≈ Cu(K2)-CeO<sub>2</sub>/CNT. As long as the selectivity to CO<sub>2</sub> is concerned, it is observed that it can reach nearly 100% before complete CO conversion, and that rapidly decreases with increasing reaction temperature. Thus, the variation in the temperature of maximum conversion of the catalysts with different K content implies that the presence of K affects the characteristics of the active phase for CO oxidation that is commonly considered to be Cu<sup>+</sup> species. Furthermore, it seems that there is an optimum K loading, around 1 wt %, that shows the best performance with a wider temperature range for CO conversion with good selectivity to CO<sub>2</sub>. This goes in line with previous suggestions that residual K<sup>+</sup> influence the physicochemical and catalytic properties of CeO<sub>2</sub> and CuO/CeO<sub>2</sub> systems.<sup>22,32</sup> It was shown that K with an appropriate content was beneficial to alleviate the adsorption of CO<sub>2</sub> and H<sub>2</sub>O on the reaction sites and improve the catalytic performance in preferential oxidation of CO in excess of hydrogen.

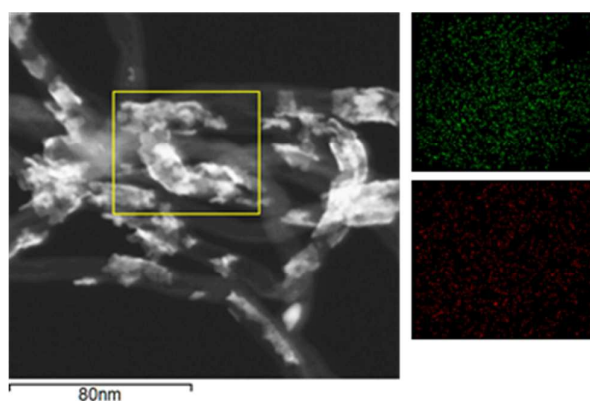


Figure 7. Dark-field STEM image of Cu(K1)-CeO<sub>2</sub>/CNT with corresponding EDS elemental maps of the highlighted area showing the chemical distribution of Ce (green) and Cu (red) for two different areas.

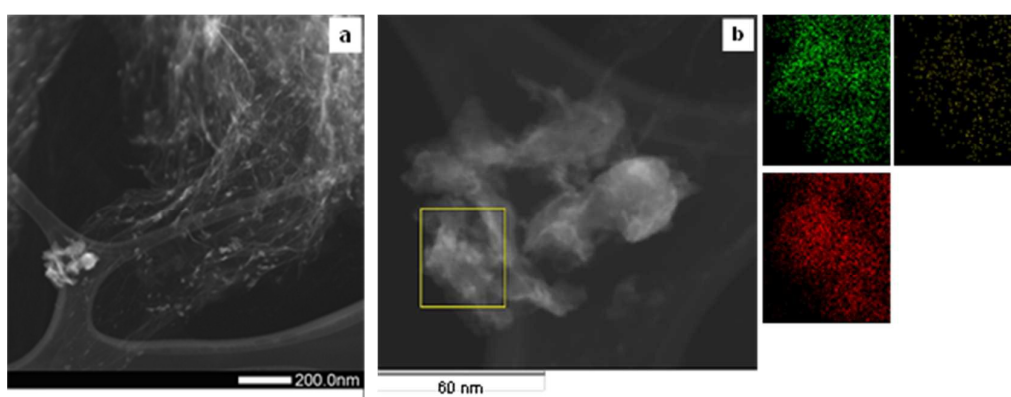


Figure 8. (a) ADF-STEM image of Cu(K1)-CeO<sub>2</sub>/G sample. (b) Dark-field STEM image with corresponding EDS elemental maps of the highlighted area showing the chemical distribution of Ce (green) and Cu (red) and K (yellow).

The CeO<sub>2</sub> crystallite size does not vary significantly with K loading as measured by XRD (ESI, Figure S2 and Table S1). However, from the TEM-STEM-EDS study some inferences were obtained. For the highest K loading, Cu(K2)-CeO<sub>2</sub>/CNT (Figure 10 and ESI, Figure S3), part of the Cu is still homogeneously distributed over CeO<sub>2</sub>, but there is an increase in the proportion of Cu-rich areas. Moreover, the Cu-CeO<sub>2</sub> domains seem to be more agglomerated and not well dispersed over the CNT support. Potassium seems to be mostly present on the Cu-CeO<sub>2</sub> dispersed areas. In addition, the effect of K loading on the catalysts properties was also detected by H<sub>2</sub>-TPR. By increasing the K content, the reduction peaks shifted to higher temperatures (Figure 5d), and the TPR profile was similar to that for the potassium free Cu-CeO<sub>2</sub>/CNT sample (Figure 5b). This is in agreement with the increase in the proportion of Cu-rich areas observed by TEM. However, deposition of non-dissolved K on the CeO<sub>2</sub> surface could also take place, as it has been proposed for Na in Ni/CeO<sub>2</sub> systems.<sup>19</sup>

#### X-ray Photoelectron Spectroscopy (XPS)

There seems to be agreement in the literature that the CO-PROX reaction occurs at the CuO-CeO<sub>2</sub> interface.<sup>33,34</sup> The reaction route mainly involves the chemisorption of CO on Cu<sup>+</sup> species stabilized on the CuO-CeO<sub>2</sub> interface and the oxidation of chemisorbed CO by the interface lattice oxygen. While, the role of ceria is to provide the oxygen source through a Ce<sup>4+</sup>/Ce<sup>3+</sup> cycle. Then, in order to shed some light on the effect of K on the catalytic behaviour, XPS analyses were performed to study the oxidation states of the surface species present on the catalysts. First, the K 1s region at 292-296 eV did not displayed any contribution for any of the measured Cu(Kx)-CeO<sub>2</sub>/CNT samples probably due to the low amount of K introduced. Therefore, the spectra for the Ce 3d, Cu 2p<sub>3/2</sub> and O 1s levels were analysed. The spectra for the Ce 3d region were deconvoluted into 8 peaks<sup>31,35,36</sup> with the assignments defined in Figure 11. Both Ce<sup>4+</sup> and Ce<sup>3+</sup> species were present in the catalysts surface, as the characteristic multiplets of 3d<sub>5/2</sub> and 3d<sub>3/2</sub> core holes were observed. The values for surface relative amount of Ce<sup>3+</sup>, estimated considering the relative area of *u'* and *v'* peaks to the area of Ce 3d region, are reported in Table 2. It can be observed that the contribution of Ce<sup>3+</sup> to the overall spectra is in the 0.17-0.22 range, and

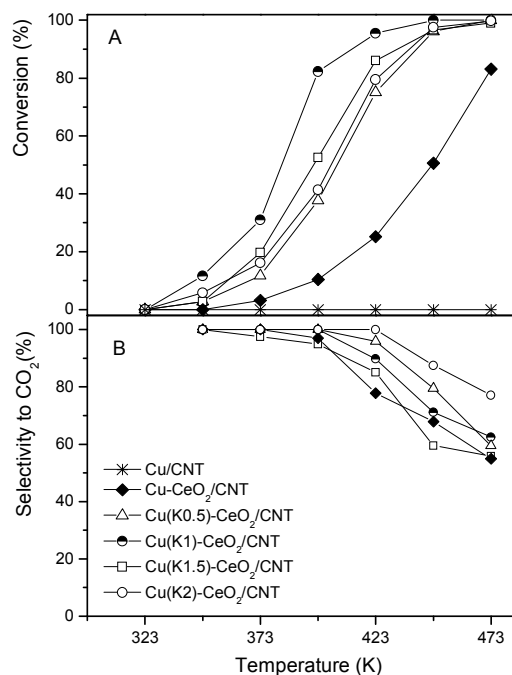


Figure 9. Plots of (A) CO conversion and (B) CO<sub>2</sub> selectivity versus temperature of CO-PROX reaction over the K-promoted series of catalysts supported on CNT. Reaction conditions as indicated in the Experimental section, CO/O<sub>2</sub> = 1.

slightly higher for Cu(K0.5)-CeO<sub>2</sub>/CNT and Cu(K1)-CeO<sub>2</sub>/CNT. The stabilization of Ce<sup>3+</sup> defects on the surface can be explained by the small ceria particle size of the supported samples. Moreover, the higher Ce<sup>3+</sup> concentration in Cu(K0.5)-CeO<sub>2</sub>/CNT and Cu(K1)-CeO<sub>2</sub>/CNT suggests the presence of copper and/or potassium ions as dopants into the ceria, this inducing additional Ce<sup>3+</sup> and oxygen vacancies.<sup>37,38</sup>

It is evident from Figure 12 that part of the surface copper species is in the reduced Cu<sup>+</sup> state due to the strongest 2p<sub>3/2</sub> peak at 932.5 eV.<sup>39,40</sup> However, the broad shake-up peak at 942.7 eV and the asymmetry of the main peak with apparent shoulders at higher binding energy, 933.4 eV, for all the samples point to the predominant presence of CuO. An accurate quantitative analysis of Cu oxidation states could not be established not only because of the low signal to noise ratios due to the rather low surface Cu content of the supported catalysts, but also the possible self-reduction of highly dispersed Cu species as a result of exposure to X-rays. However, a comparison of the ratio of intensities of satellite peaks to those of principal peaks ( $I_{\text{sat}}/I_{\text{pp}}$ ) can provide valuable information of reduced copper species. It is known that this  $I_{\text{sat}}/I_{\text{pp}}$  ratio is 0.57 for Cu<sup>2+</sup> species.<sup>41</sup> Therefore, the values of relative intensity of the shake-up to the main 2p<sub>3/2</sub> lines reported in Table 2 suggest the existence of a small amount of partially reduced copper species. It was not possible to distinguish between Cu(0) and CuO based on Cu 2p<sub>3/2</sub> photoelectron spectra due to the proximity of their respectively binding energies. An attempt to analyse the Cu L<sub>3</sub>M<sub>45</sub>M<sub>45</sub> Auger transition was neither successful. The presence of partially reduced copper species in CuO/CeO<sub>2</sub> catalysts has also been reported by other groups.<sup>39,41</sup> To explain this, well-dispersed copper oxide clusters strongly interacting with ceria or the substitution at their interface have been proposed.<sup>36,42</sup> The higher content of reduced copper species (mainly Cu<sup>+</sup>) induced in Cu(K1)CeO<sub>2</sub>/CNT, as the direct comparison of ratio of peak intensities suggests, is in agreement with the higher Ce<sup>3+</sup> concentration and reflects the ability for the redox cycle between copper and ceria. Thus, reduced Cu<sup>+</sup> species can be viewed as a good indication of a favourable synergetic interaction between copper and ceria in Cu–O–Ce sites that are proposed as the main active site for PROX reaction.

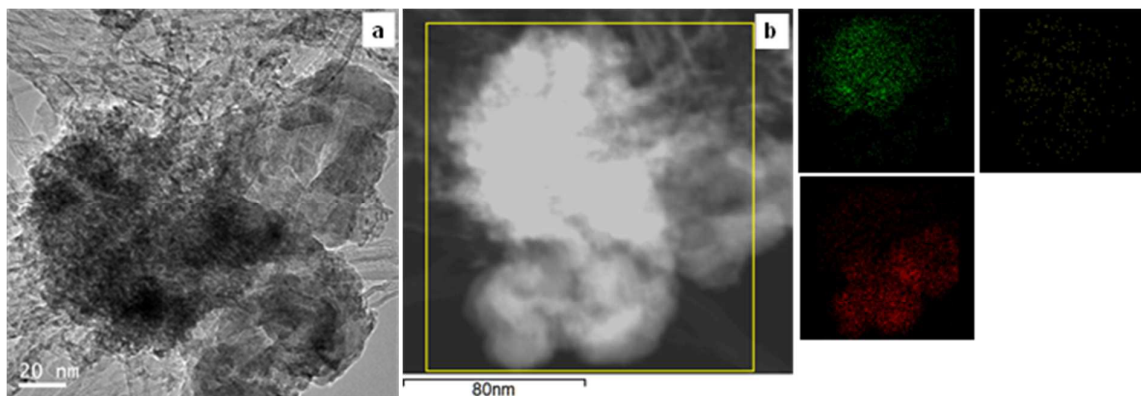


Figure 10. (a) TEM image of Cu(K2)-CeO<sub>2</sub>/CNT sample. (b) Dark-field STEM image with corresponding EDS elemental maps of the highlighted area showing the chemical distribution of Ce (green) and Cu (red) and K (yellow).

Table 2. XPS results of the catalysts supported on CNT.

Catalyst	Cu/Ce	Ce/C	Ce <sup>3+</sup> /Ce <sub>tot</sub>	O <sub>latt</sub> /O <sub>tot</sub>	I <sub>sat</sub> /I <sub>pp</sub>
CeO <sub>2</sub> /CNT		0.0049	0.17	0.39	
Cu-CeO <sub>2</sub> /CNT	0.80	0.0055	0.18	0.40	0.56
Cu(K0.5)-CeO <sub>2</sub> /CNT	0.62	0.0058	0.22	0.40	0.51
Cu(K1)-CeO <sub>2</sub> /CNT	0.61	0.0070	0.21	0.32	0.46
Cu(K1.5)-CeO <sub>2</sub> /CNT	0.47	0.0057	0.19	0.37	0.55
Cu(K2)-CeO <sub>2</sub> /CNT	0.50	0.0069	0.18	0.39	0.48

Finally, Figure 13 displays the core level spectra of the O 1s region for the samples supported on CNT. It is apparent that three O 1s components can be included in CeO<sub>2</sub>/CNT catalyst (Figure 8b). A peak at 528.9 eV is characteristic of lattice oxygen of metal oxides, a peak at around 531 eV is assigned to adsorbed oxygen and the additional last peak at higher binding energy (532.4 eV) can be assigned to surface defective Ce species in CeO<sub>2</sub> as already reported.<sup>36,39</sup> But, some small contribution of the oxygen groups present on the CNT surface (Figure 13a, O/C ratio for original CNT is 0.015) has to be considered at the higher BE side. After the addition of copper and potassium, these peaks are also observed. However, variations on the relative intensity of the components with increasing K content are evident. So, the relative intensity of the first component to the total O 1s peak (denominated as O<sub>latt</sub>/O<sub>total</sub>) was calculated and listed in Table 2. The O<sub>latt</sub>/O<sub>total</sub>

decreases for Cu(K1)-CeO<sub>2</sub>/CNT and Cu(K1.5)-CeO<sub>2</sub>/CNT and for higher K contents increases to values similar to those for the non-promoted catalysts, i.e. 0.40. The relatively lower O<sub>latt</sub>/O<sub>total</sub> for Cu(K1)-CeO<sub>2</sub>/CNT and Cu(K1.5)-CeO<sub>2</sub>/CNT suggests the presence of more Ce<sup>3+</sup> surface defects that are accompanied by the formation of oxygen vacancies. This finding correlates well with the higher Ce<sup>3+</sup>/Ce<sub>total</sub> ratio and the H<sub>2</sub>-TPR results. Then, with a weaker O<sub>latt</sub> peak, this catalyst is expected to have a better capacity for oxygen storage. Hence, the general trend of the lattice oxygen intensity with the change of K content determined by XPS is consistent with the order of catalytic performance (Fig. 9). It is well known that the oxygen storage capacity and the reactivity of lattice oxygen are important to obtain a highly active catalyst for CO oxidation.<sup>33,42</sup> The presence of defect sites (oxygen vacancies) from Cu substitutions increases the relative freedom

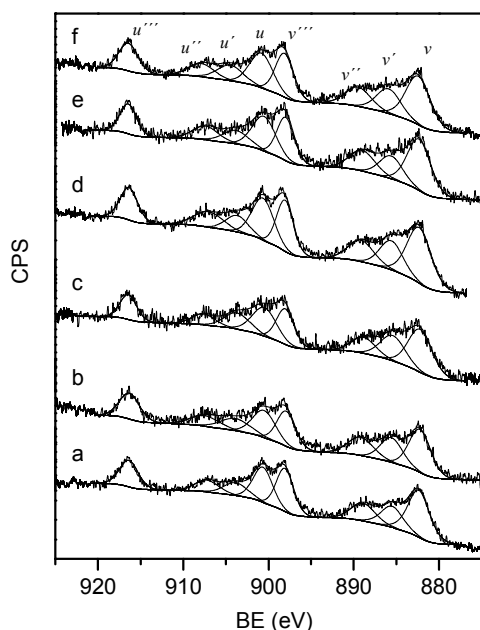


Figure 11. Ce 3d core level spectra of samples: a) CeO<sub>2</sub>/CNT, b) Cu-CeO<sub>2</sub>/CNT, c) Cu(K0.5)-CeO<sub>2</sub>/CNT, d) Cu(K1)-CeO<sub>2</sub>/CNT, e) Cu(K1.5)-CeO<sub>2</sub>/CNT, f) Cu(K2)-CeO<sub>2</sub>/CNT.

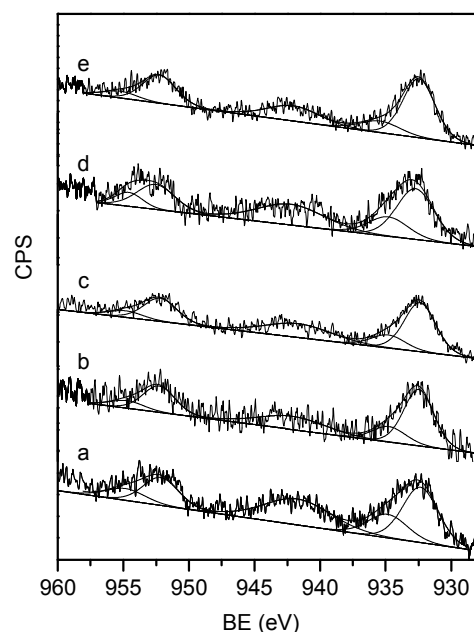


Figure 12. Cu 2p core level spectra of samples: a) Cu-CeO<sub>2</sub>/CNT, b) Cu(K0.5)-CeO<sub>2</sub>/CNT, c) Cu(K1)-CeO<sub>2</sub>/CNT, d) Cu(K1.5)-CeO<sub>2</sub>/CNT, e) Cu(K2)-CeO<sub>2</sub>/CNT.

movement of lattice oxygen and consequently enhances the oxygen mobility. It has been proposed that the addition of  $\text{Na}^+$ , within the solubility limit of 2 wt %, displaces  $\text{Ce}^{4+}$  in the  $\text{CeO}_2$  lattice, generating oxygen vacancies and thereby increasing oxygen mobility in  $\text{Ni}/x\text{Na}/\text{CeO}_2$  catalyst for the water-gas shift reaction.<sup>19</sup>

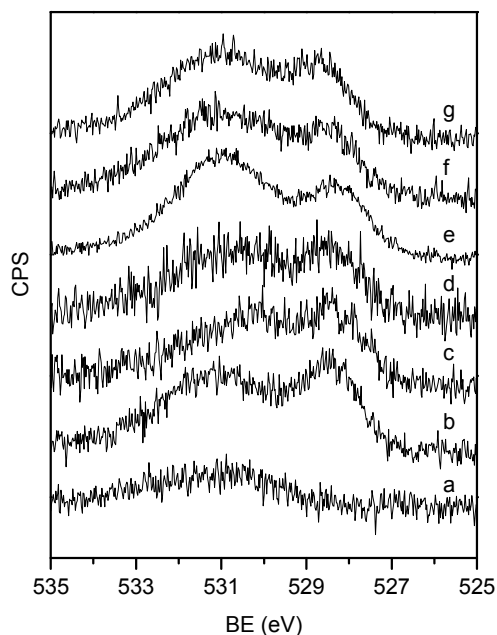


Figure 13 O 1s core level spectra of samples: a) CNT, b)  $\text{CeO}_2/\text{CNT}$ , c)  $\text{Cu-CeO}_2/\text{CNT}$ , d)  $\text{Cu(K0.5)-CeO}_2/\text{CNT}$ , e)  $\text{Cu(K1)-CeO}_2/\text{CNT}$ , f)  $\text{Cu(K1.5)-CeO}_2/\text{CNT}$ , g)  $\text{Cu(K2)-CeO}_2/\text{CNT}$ .

### Role of K doping

The activity obtained with the studied catalysts is in agreement with the characterization results and confirm the relevance of a good dispersion of ceria on the support to give a better contact with the Cu active phase. Addition of K in an appropriate amount seems to favour this Cu-Ce interaction or synergistic effect between CuO and  $\text{CeO}_2$  producing better Cu+ sites for CO adsorption. According to XRD,  $\text{H}_2$ -TPR and XPS results, it is evident that the easily reducible and highly dispersed active copper oxide species which interacts strongly with ceria is the key to achieving superior catalytic performance. The ability of potassium to stabilize cuprous ions has been reported previously even on unsupported copper catalysts for the synthesis of methanol from carbon monoxide and hydrogen.<sup>43</sup> However, the electron-donor character of K can be a factor to take also into account. This electron donating effect has been regarded as the factor that improved the competitive adsorption and activation of oxygen molecules on Ru metal surface at lower temperatures by weakening the CO adsorption and favouring the CO oxidation reaction at lower temperatures.<sup>21</sup> Similar modifications in the nature of the adsorption of CO and  $\text{O}_2$  on our materials could be

proposed. In addition, comparing the catalysts supported on the two carbon materials, the better results of the K promotion on CNT could be related to the electron conducting character of the CNT that could facilitate the transfer of electrons from potassium.

### Conclusions

We have developed highly active Cu-Ce carbon nanotubes supported catalysts for the PROX reaction. Cerium oxide (20 wt %) has been dispersed over commercial carbon nanotubes and a lab-prepared graphene oxide. The results indicate that the morphology and the surface chemistry of the supports play an important role on the dispersion of ceria. XRD and TEM studies have confirmed the small crystal size (4-6 nm) and high dispersion of  $\text{CeO}_2$  over the CNT support in comparison with the graphene. Comparing the two supports, the better ceria dispersion afforded on CNT resulted in a better interaction Cu-ceria, this leading to a better catalytic performance. Promotion with K was studied over the two carbon supports, carbon nanotubes and graphene. It was observed that the activity achieved over the former catalyst was better, which can be ascribed to the better dispersion of ceria over the carbon nanotubes, despite their lower surface area, favouring a superior Cu-Ceria interaction. The influence of different K loadings was also studied over the CNT based catalysts. An optimum K loading (around 1 wt %) resulted in an increase of the catalysts activity at lower temperature. Increasing the potassium loading, the catalytic performance become worse and approaches that for the K-free catalyst. As demonstrated by XPS, promotion with K seems to favour the generation of oxygen vacancies and the synergistic effect between Cu and  $\text{CeO}_2$ . It can be concluded that the presented results showed that promotion with K is a promising method to improve the performance of Cu-Ceria systems in the CO-PROX reaction.

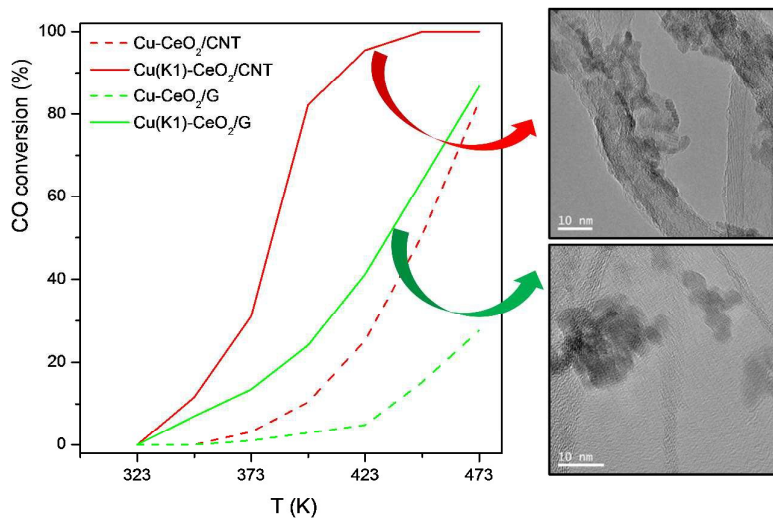
### Acknowledgements

Financial support of the Spanish Ministerio de Economía y Competitividad by projects CTQ2014-52956-C3-2-R and 3-R is recognized and from CONICYT-Chile for FONDECYT project 3130483.

### References

- 1 M.A. Peña, J.P. Gómez, J.L.G. Fierro, *Appl. Catal. A: Gen.*, 1996, **144**, 7-57.
- 2 N. Bion, F. Epron, M. Moreno, F. Mariño, D. Duprez, *Topics Catal.*, 2008, **51**, 76-88
- 3 A. Martínez-Arias, A.B. Hungria, G. Munuera, D. Gamarra, *Appl. Catal. B: Environ.*, 2006, **65**, 207-216.

- 4 L. Kundakovic, M. Flytzani-Stephanopoulos, *Appl. Catal. A: Gen.*, 1998, **171**, 13–29
- 5 A. Iriondo, V.L. Barrio, J.F. Cambra, P.L. Arias, M.B. Guemez, M.C. Sanchez-Sanchez, R.M. Navarro, J.L.G. Fierro, *Int. J. Hydrogen Energy*, 2010, **35**, 11622–11633
- 6 H. Zhu, W. Wang, R. Ran, Z. Shao, *Int. J. Hydrogen Energy*, 2013, **38**, 3741–3749.
- 7 J. Beckers, G. Rothenberg, *Green Chem.*, 2010, **12**, 939–948.
- 8 Z. Wu, H. Zhu, Z. Qin, H. Wang, L. Huang, J. Wang, *Appl. Catal. B: Environ.*, 2010, **98**, 204–212
- 9 C.T. Peng, H.K. Lia, B.J. Liaw, Y.Z. Chen, *Chem. Eng. J.*, 2011, **172**, 452–458.
- 10 E. Moretti, L. Storaro, A. Talona, P. Riello, A.I. Molina, E. Rodríguez-Castellón, *Appl. Catal. B: Environ.*, 2015, **168–169**, 385–395.
- 11 J. Li, Y. Han, Y. Zhu, R. Zhou, *Appl. Catal. B: Environ.*, 2011, **108–109**, 72–80.
- 12 J.L. Ayastuy, E. Fernández-Puertas, M.P. González-Marcos, M.A. Gutiérrez-Ortiz *Int. J. Hydrogen Energy*, 2012, **37**, 7385–7397.
- 13 X. Guo, J. Li, R. Zhou, *Fuel*, 2016, **163**, 56–64.
- 14 R. Buitrago, J. Ruiz, J. Silvestre-Albero, A. Sepúlveda-Escribano, F. Rodríguez-Reinoso, *Catal. Today*, 2012, **180**, 19–24.
- 15 E. Jardim, M. Goncalves, S. Rico-Francés, A. Sepúlveda-Escribano, J. Silvestre-Albero, *Appl. Catal. B: Environ.*, 2012, **113**, 72–78.
- 16 Y. Gao, K. Xie, W. Wang, S. Mi, N. Liu, G. Pan, W. Huang, *Catal. Sci. Technol.*, 2015, **5**, 1568–1579.
- 17 S. Zeng, L. Zhang, N. Jiang, M. Gao, X. Zhao, Y. Yin, H. Su, *J. Power Sources*, 2015, **293**, 1016–1023.
- 18 P. Serp, E. Castillejos, *ChemCatChem.*, 2010, **2**, 41–47.
- 19 M.L. Ang, U. Oemar, E. T. Saw, L. Mo, Y. Kathiraser, B. H. Chia, S. Kawi, *ACS Catal.*, 2014, **4**, 3237–3248.
- 20 M.L. Ang, U. Oemar, Y. Kathiraser, E.T. Saw, C.H.K. Lew, Y. Du, A. Borgna, S. Kawi, *J. Catal.*, 2015, **329**, 130–143.
- 21 T. Niu, C.X. Wang, L.H. Zhang, Y. Liu, *Int. J. Hydrogen Energy*, 2013, **38**, 7801–7810.
- 22 Z. Liu, R. Zhou, X. Zheng, *Int. J. Hydrogen Energy*, 2008, **33**, 791–796.
- 23 H. Tanaka, M. Kuriyama, Y. Ishida, S. Ito, T. Kubota, T. Miyao, S. Naito, K. Tomishige, K. Kunimori, *Appl. Catal. A: Gen.*, 2008, **343**, 125–133.
- 24 E. Asedegbega-Nieto, M. Perez-Cadenas, M.V. Morales, B. Bachiller-Baeza, E. Gallegos-Suarez, I. Rodriguez-Ramos, A. Guerrero-Ruiz, *Diam. Relat. Mater.*, 2014, **44**, 26–32.
- 25 K.V.R. Chary, G.V. Sagar, D. Naresh, K.K. Seela, B. Sridhar, *J. Phys. Chem. B*, 2005, **109**, 9437–9444
- 26 M.F. Luo, Y.J. Zhong, X.X. Yuan, X.M. Zheng, *Appl. Catal. A*, 1997, **162**, 121.
- 27 X.B. Li, X.Y. Quek, D.A.J.M. Ligthart, M.L. Guo, Y. Zhang, C. Li, Q.H. Yang, E.J.M. Hensen, *Appl. Catal. B: Environ.*, 2012, **123**, 424–432.
- 28 J. Beckers, G. Rothenberg, *Dalton Trans.*, 2008, 6573–6578.
- 29 D. Gamarra, A. Hornés, Zs. Koppány, Z. Schay, G. Munuera, J. Soria, A. Martínez-Arias, *J. Power Sources*, 2007, **169**, 110.
- 30 J. Astudillo, G. Águila, F. Díaz, S. Guerrero, P. Araya, *Appl. Catal. A: Gen.* 2010, **381**, 169–176.
- 31 S. Sun, D. Mao, J. Yu, Z. Yang, G. Lua and Z. Ma, *Catal. Sci. Technol.*, 2015, **5**, 3166.
- 32 X. Zheng, X. Zhang, S. Wang, X. Wang, S. Wu, *J. Nat. Gas Chem.*, 2007, **16**, 179–185.
- 33 G. Sedmak, S. Hocevar, J. Levec, *J. Catal.*, 2003, **213**, 135–150.
- 34 A. Martínez-Arias, M. Fernández-García, O. Gálvez, J.M. Coronado, J.A. Anderson, J.C. Conesa, J. Soria, G. Munuera, *J. Catal.*, 2000, **195**, 207.
- 35 I. Jiménez-Morales, F. Vila, R. Mariscal, A. Jiménez-López, *Appl. Catal. B: Environ.*, 2012, **117**, 253–259.
- 36 S. Zeng, Y. Wang, S. Ding, J.J.H.B. Sattler, E. Borodina, L. Zhang, B.M. Weckhuysen, H. Su, *J. Power Sources*, 2014, **256**, 301–311.
- 37 M. Yang, S. Li, Y. Wang, J.A. Herron, Y. Xu, L.F. Allard, S. Lee, J. Huang, M. Mavrikakis, M. Flytzani-Stephanopoulos, *Science*, 2014, **346**, 1498–1501.
- 38 A.B. Dongil, L. Pastor-Pérez, A. Sepúlveda-Escribano, P. Reyes, *Appl. Catal. A: Gen.*, 2015, **505**, 98–104.
- 39 L. Qi, Q. Yu, Y. Dai, C.J. Tang, L.J. Liu, H.L. Zhang, F. Gao, L. Dong, Y. Chen, *Appl. Catal. B: Environ.*, 2012, **119–120**, 308–320.
- 40 C. Tang, J. Sun, X. Yao, Y. Cao, L. Liu, C. Ge, F. Gao, L. Dong, *Appl. Catal. B: Environ.*, 2014, **146**, 201–212.
- 41 G. Avgouropoulos, T. Ioannides, *Appl. Catal. A: Gen.*, 2003, **244**, 155–167.
- 42 W. Liu, M. Flytzani-Stephanopoulos, *J. Catal.*, 1995, **153**, 304.
- 43 G.R. Sheffer, T.S. King, *J. Catal.*, 1989, **115**, 376–387.



Improved performance of catalysts promoted with K was obtained in the CO-PROX reaction